Determination of Oil/Water Saturation Functions of Chalk Core Plugs From Two-Phase Flow Experiments

Niels Bech, SPE, **Dan Olsen,** SPE, and **C.M. Nielsen,** Geological Survey of Denmark and Greenland (GEUS)

Summary

A new procedure for obtaining oil/water saturation functions, i.e., capillary pressure and relative permeability, of tight core samples uses the pronounced end effect present in flooding experiments on such material. In core material with high capillary pressure, the end effect may allow determination of the saturation functions for a broad saturation interval. A complex coreflooding scheme provides the fluid distributions and production data from which the saturation functions are computed for both drainage and imbibition by a least-squares technique. A chemical shift NMR technique is used for fluid distribution determination. An undesirable interdependency of the saturation functions is avoided by their calculation from different data sets. Killough's method is employed to account for the scanning effect in hysteresis situations for both capillary pressure and relative permeability. The procedure is demonstrated on chalk samples from the North Sea. The experimental time is intermediate between the centrifuge and porous plate methods.

Introduction

Petrophysical parameters are an integrated part of every simulation study concerning displacement processes in porous media. A prerequisite for meaningful modeling is reliable petrophysical data. Simulations and models rapidly evolve in the direction of more details and greater precision, and the underlying petrophysical data should evolve accordingly. Several workers have presented methods utilizing coreflooding techniques in combination with computer simulations to determine saturation functions of rock samples.[1-9] The aim of the present work is to develop an experimental method, which is particularly suitable for determination of the oil/water capillary pressure and relative permeability for samples of chalk for both drainage and imbibition. Inherently, chalk has high capillary pressure, and laboratory determinations of saturation functions on such material are complicated by strong scale effects, particularly by the capillary end effect. This capillary retention of the wetting phase in displacement experiments results in a saturation gradient through the core sample. Although being a problem in many traditional core analyses, the end effect actually contains detailed information about the saturation functions of the sample, and can cover a large saturation interval. The idea of the work is to make use of this information to calculate relative permeability functions and capillary pressure curves.

Conventional methods for determination of saturation functions are mainly developed for rocks of lower capillary pressure and higher mechanical strength than chalk, and their application to chalk may be questionable. The mercury injection method for capillary pressure determination uses a fluid system with wetting characteristics and surface tension much different from the oil/water fluid system of an oil reservoir. The centrifuge method for determination of capillary pressure is largely unsuitable due to the low mechanical strength of chalk, as well as the difficulty of obtaining the necessary high rotational speed. In addition, no general agreement exists on the flow equations for deriving capillary pressure from centrifuge data.[10-13] The porous plate method for determination of capillary pressure appears to be valid, but is extremely time consuming for low permeability materials. The steady-state and unsteady-state methods for determination of relative permeability are experimentally viable, but must be coupled to computational procedures to account for the saturation gradients caused by capillary pressure. Classical Buckley-Leverett theory does not account for capillary pressure.

The method to be presented is based on a parameter estimation technique, utilizing saturation data obtained from a complex experimental coreflooding procedure developed by Nielsen *et al.*[14] It uses the prominent end effect that is caused by the strong capillary forces of rocks with low permeability and allows calculation of both drainage and imbibition saturation functions. The method assumes capillary continuity of the fluid phases, and homogeneity of the sample with respect to the saturation functions.

Experimental Technique

The method depends on experimental data on the distribution of fluids during flooding experiments. A one-dimensional (1D) nuclear magnetic resonance (NMR) imaging technique is used for quantification of the fluid distribution.[15] This technique is restricted to rocks with NMR spin-spin relaxation constants above approximately 6 ms, encompassing many types of limestone, but excluding nearly all types of sandstone. Fortunately, the computational method is not dependent on a specific technique for quantifying the fluid distribution. Gamma-ray attenuation,[16] x-ray computerized tomography (CT) scanning,[3,17] or microwave scanning techniques,[18] may be suitable.

Sample Material. The material used in the experimental work is chalk of Maastrichtian age from the Dan field in the Danish sector of the North Sea known to comply with the NMR requirements.[15] Results are presented for two samples. Both are cylindrical 38 mm plug samples, drilled with the cylinder axis parallel to any visible bedding or layering, to minimize effects of sample inhomogeneity on the flooding experiments. 1D signal intensity profiles indicate that samples M113 and M16H are homogeneous within experimental scatter, while two-dimensional (2D) spin-echo images reveal the presence of minor hairlines. The samples were cleaned by Soxhlet extraction with methanol and toluene prior to the flooding experiments. The samples are strongly water-wet. Basic parameters for the samples are given in **Table 1**.

Fluid Data. A synthetic formation brine with a salinity of 7% was used. The brine is similar in composition to formation water from the Dan field. *N*-decane was used as the nonwetting oil phase. A prerequisite for the parameter estimation technique and the NMR measurements is that the fluid system can be described as a two-phase system. It is thus essential to avoid the presence of a free-gas phase. This was accomplished by degassing of all fluids.

Flooding Experiments. Information for calculation of both drainage and imbibition capillary pressure functions, as well as drainage and imbibition relative permeability functions is obtained from a complex coreflooding procedure. The procedure consists of a sequence of five flooding experiments as follows:

- Step 1: Threshold pressure experiment.
- Step 2: Transient flow drainage experiment.
- Step 3: Stationary flow drainage experiment.
- Step 4: Stationary flow internal imbibition experiment.
- Step 5: Forced flow imbibition experiment.

This paper (SPE 60769) was revised for publication from paper SPE 49325, prepared for presentation at the 1998 SPE Annual Technical Conference and Exhibition, New Orleans, 27–30 September 1998. Original manuscript received for review 19 January 1999. Revised manuscript received 4 November 1999. Paper peer approved 15 November 1999.

TABLE 1– NMR PARAMETERS

Sample (ID)	M113	M16H
T_1 (ms)		500
T_2 (ms)		10.6
NMR profile length (mm)	90	90
NMR profile resolution (mm/pixel)	0.35	0.35
NMR profile acquisition time (hour)	6	9
NMR frequency window for integration (Hz)	500	500
t_r (s)	6.0	9.0
No. of t_e value	7	7
Minimum t_e value (ms)	2.5	2.5
Duration of rf pulses (ms)	0.1	0.1
$\rho_{p,w}$	0.9759	0.9759
$\rho_{p,o}$	1.0185	1.085
Reproducibility (1 s.d.) (p.u.)	2	2
Accuracy (pixel saturation) (p.u.)	5	5
Accuracy (bulk saturation) (p.u.)	2	2

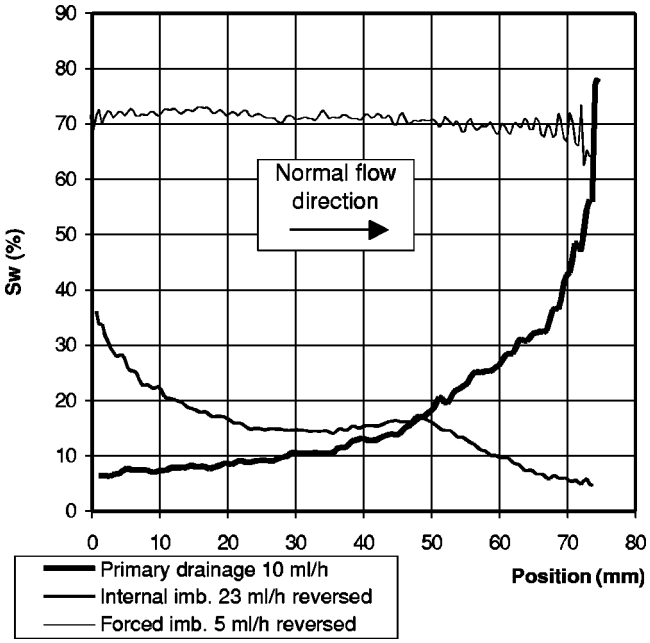

Fig. 1–Measured saturation profiles for sample M113.

The steady-state situation at the end of a primary drainage experiment allows calculation of the drainage capillary pressure and the drainage oil relative permeability. The water relative permeability is calculated from the unsteady-state data obtained during the transient part of this experiment. After a flow reversal, a new end effect develops at the opposite end of the core by an internal imbibition process, which at steady state allows calculation of the spontaneous imbibition capillary pressure and the imbibition oil relative permeability. Following a change from oilflooding to waterflooding, the forced imbibition capillary pressure is calculated from transient pressure drop measurements.

A nonmagnetic Hassler-type core holder connected to a Mobile Flooding Unit[19] is used to allow NMR measurement during the experimental steps while sustaining fluid flow through the sample.

Step 1: Threshold Pressure Experiment. The sample is saturated with brine, and a drainage experiment is set up with a very slow linear upramping of the inlet oil pressure, while displaced fluid volume is recorded. A plot of the inlet oil pressure vs displaced fluid volume shows a distinct break at the point when the oil phase enters the sample. The inlet pressure at this point is the threshold pressure p_{th}.

Step 2: Transient Flow Drainage Experiment. After the threshold pressure experiment, the sample is cleaned and resaturated with brine. Then, a transient flow drainage experiment is conducted at constant rate q_o with monitoring of fluid production and $\Delta p_{o,T}$ as a function of time. The data are used for calculation of the drainage relative permeability to water, k_{rw}^{dr}. This experiment is similar to a conventional unsteady-state Buckley-Leverett experiment, but the use of the resulting data set is different.

Step 3: Stationary Flow Drainage Experiment. During the transient flow drainage experiment the flow is sustained at controlled temperature and flow rate until a stable $\Delta p_{o,T}$ is obtained, and until water production has ceased. At steady state, a stable fluid saturation gradient is present in the sample (see, e.g., **Fig. 1**), and the stationary flow drainage experiment is conducted, with monitoring of the S_w profile. The data set is used for calculation of k_{ro}^{dr} and p_c^{dr}. The fluid saturation profile is measured by NMR.

Step 4: Stationary Flow Internal Imbibition Experiment. The oil flow direction is now reversed and the water contained in the end effect is displaced through the sample towards the former inlet, where a new end effect evolves due to the capillary retention of the water. By this flow reversal one part of the sample undergoes a drainage process and another an imbibition process. The buildup of the new end effect follows a spontaneous imbibition process because the oil pressure is higher than the water pressure during the displacing of the end effect. The flow rate must be large enough to create a water production from the sample. If the flow rate is insufficient to cause water production, the water saturation measured in the downstream part of the sample may be controlled by the availability of water rather than by the bounding imbibition capillary pressure curve of the sample, leading to erroneous calculation of $p_{c,spt}^{imb}$ and dependent parameters. The stationary flow internal imbibition data set is measured, when $\Delta p_{o,T}$ is stable, and water production has ceased (see, e.g., Fig. 1). Again, NMR is used to monitor the S_w profile. The data are used for calculation of k_{ro}^{imb} and k_{ro}^{imb}, together with the capillary pressure scanning parameter ϵ.

Step 5: Forced Flow Imbibition Experiment. In the last experiment step, a forced imbibition process is produced in the sample by flooding the sample with brine. During the transient flooding period $\Delta p_{w,T}$, as a function of time, is measured. When a static flow situation is reached, NMR is used to monitor the water saturation profile from which the value of irreducible oil saturation is determined (see, e.g., Fig. 1). The data set is used to calculate $p_{c,\text{forced}}^{imb}$.

NMR Measurements

Hardware. A 4.7 T SISCO experimental NMR scanner is used for the NMR work. It is equipped with a 130-mm-diam insert gradient set, capable of producing magnetic gradient up to 100 mT/m along any of three orthogonal directions. The gradient rise rate is 2×10^5 mT/m·s. A radio-frequency (rf) coil of a slotted tube resonator design is used. It has a good signal homogeneity until a maximum length of 90 mm.

Pulse Sequence. The objective of the NMR measurements is to obtain fluid saturation information, that is spatially resolved along the direction of fluid flow through a sample. This is accomplished by using a one-dimensional chemical shift pulse sequence named *TST*.[15] Assuming homogeneity of the sample, the flooding experiments are essentially 1D experiments, and the use of a 1D pulse sequence is appropriate.

In the investigated samples the contents of paramagnetic and ferromagnetic minerals are low, and the main magnetic field B_0, has good homogeneity across the sample. The linewidth of the oil and water resonances lies between 100 and 200 Hz full width at half maximum (FWHM), with the two resonances separated by 700 to 800 Hz. Mutual interference between the two resonances is below 5% of the total signal intensity. The interference is significantly compensated by an interference correction procedure using interference factors determined on single-fluid profiles, where mutual interference is absent.

Data Processing. A data set from the *TST* pulse sequence represents a stack of spectra at consecutive spatial positions. The following data processing steps are necessary to transform this 2D data set to a quantitative 1D saturation profile:

- Step 1: Frequency dimension elimination.
- Step 2: Relaxation correction.
- Step 3: Proton density correction.
- Step 4: Calculation of saturation.

The saturation profiles have 256 pixels (data values) and are, typically, 90 mm long. The time requirement for a high-quality saturation profile is approximately 2 hours. Compliance with t_r (repetition time), resolution, number of values for t_e (echo time), phase cycling, and spatial resolution may bring the acquisition time for a saturation profile down to 5 minutes, and still retain a fair signal-to-noise ratio. Readers interested in the NMR data processing procedure are referred to Olsen *et al.*[15]

Relaxation Correction. The effect of spin-lattice relaxation is eliminated by selecting t_r at least five times as long as the longest T_1 component of the sample. With this convention, it is assured that the error on signal intensity due to differential saturation of the NMR signals is less than 1% of the detected signals.

Spin-spin relaxation of an inhomogeneous system is a complex process, which in principle follows a multiexponential behavior according to

$$M(t)=M(t=0)\int P(a)\exp[-t/T_2(a)]\mathrm{d}a, \tag{1}$$

where $M(t)$ is the magnetization at time t, $P(a)$ is the volume probability density function for pore size a, and $T_2(a)$ is the spin-spin relaxation constant for pores of size a.[20]

The spin-spin relaxation of a sample is compensated by a relaxation modeling on an array of data sets.[9,21-24] The array of data sets is acquired, with identical acquisition parameters, except for different values of t_e. A spin–spin relaxation modeling is then performed for each pixel array, producing 1D data sets of the fitted parameters, which include the magnetization at time zero, $M(t=0)$. The t_e values of the setup are selected for optimal definition of the relaxation. Downwards, the setting of t_e is restricted by system hardware constraints. Slightly dependent on the setup, the smallest possible t_e value, $t_{e,\min}$, is 2.5 ms for the *TST* pulse sequence. The smallest t_e value is usually selected to be close to $t_{e,\min}$, in order to trace the relaxation path as close to the $M(t=0)$ condition as possible. The largest t_e value in a t_e array is usually selected to be approximately three times the anticipated single-exponential T_2 relaxation constant, at which time the magnetization $M(t)$ has declined to 5% of the $M(t=0)$ value.

An important issue is the choice of spin-spin relaxation model. Single-exponential, biexponential, and stretched-exponential models were tested by Kim *et al.*,[25] while Kenyon *et al.*[26] tested biexponential, triexponential, and stretched-exponential modeling. The conclusion of Kim *et al.* is that biexponential fitting is preferable, while Kenyon *et al.* find that stretched-exponential fitting is preferable. Working on chalk samples, Olsen[15] finds that $M(t=0)$ in chalk is confidently determined by single-exponential fitting. In the present project single-exponential modeling is used, i.e.,

$$M(t)=M(t=0)\exp(-t/T_2)+E, \tag{2}$$

where E is the signal level (noise) at $t=\infty$. For nearly all pixels the extrapolation of the fit from $M(t=t_{e,\min})$ to $M(t=0)$ is short, because the ratio $M(t=t_{e,\min})/M(t=0)$ is above 0.5. For a large majority of pixels modeling by Eq. 2 results in good precision for the estimation of $M(t=0)$. Failure to produce good fits mainly occurs at the ends of a sample, where susceptibility contrasts destroy the homogeneity of the magnetic field. These inferior fits cannot be improved by choosing another relaxation model. The validity of the single-exponential model is confirmed by good agreement [around 2 percentage units (p.u.)] between bulk saturation determinations by integration of NMR profiles and conventional methods (Dean-Stark extraction and gravimetric determination).

The success of the single-exponential model may be explained by low surface relaxivity caused by the high static magnetic field[27] and low contents of paramagnetic material,[28] which creates approximately single-exponential relaxation by fulfilling the conditions of the fast-diffusion regime.[29,30] The condition may be enhanced by an environment with relatively homogeneous pore structure.

Limitations and Accuracy of the NMR Method. Spin-spin relaxation and resolution of the NMR resonances restrict the choice of samples suitable for NMR saturation profile measurement. The samples in this work have T_2 values around 10 ms and good resolution of the NMR resonances. Comparison of the mean saturations of saturation profiles with conventional bulk saturation determinations indicates an accuracy for the NMR method of 2 p.u. on the mean saturations.[15] The accuracy of the pixel saturations is inferior, probably around 5 p.u., but dependent on the setup. The reproducibility of the pixel saturations is 2 p.u., as estimated from replicate analyses and saturation profile smoothness.

Parameter Estimation Technique

The experimental data used for the determination of the saturation functions, are the pressure data and saturation profiles obtained from the complex flooding procedure. The saturation functions are determined as analytical functions of the saturation.

The flooding experiments are divided into a drainage case and two imbibition cases. Inlet flow rates are constant within each case. The flow directions of the two imbibition cases are reversed relative to the drainage case. The origin for the length scale is the sample inlet in the drainage case. In flooding situations with reversed flow direction the origin is the sample outlet. The length scale is thus fixed relative to the sample.

Like the experimental procedure, the parameter estimation technique is divided into drainage and imbibition parts, as described below. Elaborate information on initial and boundary conditions for the mathematical model can be found in Bech *et al.*[31]

Drainage. The drainage case initial conditions correspond to a core plug saturated with water. The plug is drained by injecting oil at a constant rate. Given enough time, flooding the sample at constant rate results in a steady-state situation, where only the displacing fluid is flowing. The Darcy equation for the water phase shows that the pressure gradient in the displaced water phase is zero. In other words, the water pressure is uniform throughout the sample. If the functional relationships of relative permeability to oil and capillary pressure with respect to water saturation are known, then the water saturation profile of a horizontal core plug can be calculated from the following equation, assuming constant porosity and fluid densities:

$$\frac{\mathrm{d}S_w}{\mathrm{d}x}=-\frac{\mu_o}{kk_{ro}}\frac{q_o}{A}\frac{1}{\dfrac{\mathrm{d}p_c}{\mathrm{d}S_w}}. \tag{3}$$

The functional relationships of the oil relative permeability and the capillary pressure are assumed to be uniquely described by two sets of parameters

$$k_{ro}(S_w)=f_a(a_1,a_2,\ldots,a_{no},S_w), \tag{4}$$

$$p_c(S_w)=f_b(b_1,b_2,\ldots,b_{nc},S_w). \tag{5}$$

To determine the drainage capillary pressure and the drainage relative permeability to oil, data from the stationary flow drainage experiment is used, i.e., step 3 of the experimental procedure. In this experiment the steady-state saturation profile of the sample and the oil-phase pressure at the inlet is measured. The unknown parameters a_i, $i=1,no$ and b_i, $i=1,nc$ are determined by means of a parameter estimation technique. For a given set of coefficients a_i and b_i in Eqs. 4 and 5 the water saturation S_w, the oil relative permeability k_{ro}, and the capillary pressure p_c are calculated from Eqs. 3–5. The coefficients a_i and b_i are determined so that they minimize the following least-squares objective function

$$J_1(\overline{a},\overline{b})=\sum_{i=1}^{M}\,[S_w^C(x_i)-S_w^m(x_i)]^2F_{w1}^2+(\Delta p_{o,T}^C-\Delta p_{o,T}^m)^2F_{w2}^2$$
$$+(p_{th}^C-p_{th}^m)^2F_{w3}^2+(p_{o,\text{out}}^C-p_{o,\text{out}}^m)^2F_{w4}^2. \quad (6)$$

The squared residuals are scaled by means of weight factors F_w to make their contribution to the objective function similar in size.

The objective function Eq. 6 is minimized by use of a standard nonlinear least-square solver [MI0L2 (Ref. 32)].

In order to determine the relative permeability to water, the transient flow drainage experiment is used, i.e., step 2 of the experimental procedure. The relative permeability to water is also represented by a functional relationship of the water saturation:

$$k_{rw}(S_w)=f_c(c_1,c_2,\ldots,c_{nw},S_w). \quad (7)$$

The coefficients are determined so that they minimize the following least-squares objective function, by use of the same nonlinear least-square solver as above:

$$J_2(\overline{c})=\sum_{i=1}^{N}\,[\Delta p_{o,T}^C(t_i)-\Delta p_{o,T}^m(t_i)]^2. \quad (8)$$

For a given set of coefficients, c_i, the relative permeability to water is calculated from Eq. 7. The relative permeability to oil and the capillary pressure are known from above.

The transient part of the drainage process is computed by means of a commercial reservoir simulator [ECLIPSE 100 (Ref. 33)]. The extraction of results from the ECLIPSE output file is performed by means of software developed by Frandsen.[34] The objective function Eq. 8 is minimized by use of the nonlinear least-square solver referenced above.

Imbibition. It is assumed in the present work that the water relative permeability exhibits no hysteresis.[35,36] In other words, the relative permeability function determined for the drainage case also applies to the imbibition cases. In order to determine the imbibition part of the saturation functions, the experiment is continued in two steps:

Experimental step 4: The end effect is shifted to the opposite end of the core ($x=0$) by reversing the direction of the oil flow.

Experimental step 5: The plug is flooded by water injected through the face $x=L$.

The experiments are simulated by means of ECLIPSE.

Imbibition Case I (Experimental Step 4). The development of an end effect at the new sample outlet follows an internal imbibition process, while the old end effect is broken down by an internal drainage process. The saturation profile at the new sample outlet can be used in the calculation of the saturation functions for the imbibition process. Recall that the bounding saturation curves are obtained under the initial condition of $S_w=100\%$ and $S_w=S_{iw}$ for the drainage and imbibition processes, respectively. The reversed drainage process violates this condition and scanning curves between the bounding saturation functions will, therefore, control the process. The scanning process is described by a method developed by Killough.[36] The scanning curves are dependent on the local saturation history of the sample.

Data from the stationary flow internal imbibition experiment, i.e., experimental step 4, are used to determine the imbibition relative permeability to oil, the spontaneous part of the imbibition capillary pressure, and the scanning parameter ϵ, which controls how the primary drainage and spontaneous imbibition capillary pressure curves are weighted to form the scanning curves. In this experiment the total pressure drop and the saturation profile are measured in the steady state, which follows the reversal of the oil flow direction. The imbibition relative permeability to oil and the imbibition capillary pressure are represented by functional relationships similarly to Eqs. 4 and 5. The coefficients a_i, b_i, and ϵ are determined by the least-squares solver so they minimize the following least-square objective function:

$$J_3(\overline{a},\overline{b},\epsilon)=\sum_{i=1}^{M}\,[S_w^C(x_i)-S_w^m(x_i)]^2F_{w1}^2$$
$$+(\Delta p_{o,T}^C-\Delta p_{o,T}^m)^2F_{w2}^2. \quad (9)$$

Imbibition Case II (Experimental Step 5). Finally, in order to determine the forced part of the imbibition capillary pressure, the core plug is flooded with water in the forced flow imbibition experiment, i.e., step 5 of the experimental procedure. The capillary pressure is represented by a functional relationship similar to Eq. 5. The coefficients b_i are determined so that they minimize the following least-square objective function:

$$J_4(\overline{b})=\sum_{i=1}^{N}\,[\Delta p_{w,T}^C(t_i)-\Delta p_{w,T}^m(t_i)]^2. \quad (10)$$

Analytical Representation of Saturation Functions. The saturation functions are given as functional relationships of the water saturation.

Relative Permeabilities. The relative permeabilities are represented by power laws. The water relative permeability is given by the following expression, which is used both for drainage and imbibition, i.e., no hysteresis for the wetting-phase permeability occurs,

$$k_{rw}=c_1(S_w^{*,dr})^{c_2}, \quad (11)$$

where

$$S_w^{*,dr}=\frac{S_w-S_{iw}}{1-S_{iw}}. \quad (12)$$

The oil relative permeability is given as

$$k_{ro}=a_1(S_o^*)^{a_2}, \quad (13)$$

where hysteresis is taken into account by

$$S_o^{*,dr}=\frac{S_o}{1-S_{iw}}, \quad (14)$$

$$S_o^{*,imb}=\frac{S_o-S_{or}}{1-S_{or}-S_{iw}}. \quad (15)$$

Capillary Pressure. The capillary pressure function is divided into a drainage and an imbibition case. In the drainage case the capillary pressure is represented by the following functions:

$$p_c=\frac{b_1}{(S_w+b_2)^{b_3}}+f_1 \quad \text{if} \quad S_w\leqslant S_w^0, \quad (16)$$

$$P_c=\frac{f_2}{S_w+b_4}+f_3, \quad \text{if} \quad S_w>S_w^0. \quad (17)$$

Two pieces of the curve are used in order to permit a proper representation of cases with a point of inflection.

The parameters f_1 to f_3 are determined in such a way that the capillary pressure function Eqs. 16–17 satisfy

$$p_c(S_{iw})=p_{c,\max}, \quad (18)$$

$$p_c(S_w^0)=p_c^0, \quad (19)$$

$$p_c(1)=0, \quad (20)$$

$$\left(\frac{dp_{c,\text{Eq. 16}}}{dS_w}\right)_{S_w=S_w^0}=\left(\frac{dp_{c,\text{Eq. 17}}}{dS_w}\right)_{S_w=S_w^0}. \quad (21)$$

The capillary pressure, p_c^0 at $S_w=S_w^0$ is a sixth unknown. The expressions for the parameters f_1 to f_3 are given in Olsen *et al.*[37] We define the threshold pressure as

$$p_{th}=p_c^0+\left(\frac{dp_c}{dS_w}\right)_{S_w=S_w^0}(1-S_w^0). \quad (22)$$

In the imbibition case the capillary pressure is given as

TABLE 2– PLUG M113 PARAMETERS

$L = 74.7$ mm	$\mu_o = 0.92$ cp
$A = 1124$ mm^2	$S_{or} = 0.28$
$\phi = 0.264$	$S_{wi} = 0.064$
$k = 0.70$ mD	$S_{w,spt} = 0.68$
$C_r = 1.76 \times 10^{-3}$ atm^{-1}	$p_{c,\max} = 5.527$ atm
$\rho_w = 1.049$ g/mL	$p_{o,\text{out}} = 1.0$ atm
$\mu_w = 1.12$ cp	$p_{th} = 1.836$ atm
$C_w = 4.58 \times 10^{-5}$ atm^{-1}	$q_o^{dr} = 10.0$ mL/h
$\rho_o = 0.73$ g/mL	$q_o^{imb} = -23.0$ mL/h
$C_o = 1.16 \times 10^{-4}$ atm^{-1}	$q_w^{imb} = -5.0$ mL/h

$$p_c = \frac{e_1}{S_w + d_1} + e_2, \quad \text{if } S_w \leq S_{w,spt}, \tag{23}$$

$$p_c = e_3 (S_w - d_2)^{e_5} + e_4, \quad \text{if } S_w > S_{w,spt}. \tag{24}$$

The parameters e_1 to e_5 are determined in such a way that the capillary pressure function Eqs. 23–24 satisfy

$$p_c(S_{iw}) = p_{c,\max}, \tag{25}$$

$$p_c(S_{w,spt}) = 0, \tag{26}$$

$$p_c(1 - S_{\text{or}}) = p_{c,\min}, \tag{27}$$

$$\left(\frac{\mathrm{d}p_{c,\text{Eq. 23}}}{\mathrm{d}S_w}\right)_{S_w = S_{w,spt}} = \left(\frac{\mathrm{d}p_{c,\text{Eq. 24}}}{\mathrm{d}S_w}\right)_{S_w = S_{w,spt}}. \tag{28}$$

$S_{w,spt}$ is the saturation where the imbibition capillary pressure is zero. It is assumed here that $S_{w,spt}$ is known. The expressions for the parameters e_1 to e_5 are given in Olsen *et al.*[37]

Test of the Parameter Estimation Technique. The parameter estimation technique was tested on a numerical core plug characterized by a set of synthetic saturation functions. The drainage case and imbibition cases I and II were simulated by means of ECLIPSE. The resulting fluid saturation distributions and pressure drop curves were treated as measured experimental results in this synthetic case.

Excellent agreement was found to exist between the calculated results and the specified saturation functions demonstrating that the present procedure for calculating saturation functions from saturation profiles and production data is valid for ideal synthetic data.

It was found that it is important to know the threshold pressure. If the threshold pressure is not available the simultaneous iterations on oil relative permeability and capillary pressure may converge towards an erroneous solution. This is because the water saturation gradient, Eq. 3, is a function of the product of the oil relative permeability and the gradient of the capillary pressure with respect to water saturation. An additional fixpoint of the capillary pressure curve is needed other than the two end points.

Results and Discussion

For two plugs labeled M113 and M16H, saturation functions are presented, as determined by use of the five-step flooding procedure and the parameter estimation technique.

Plug M113. The M113 plug parameters and some experimental conditions are given in **Table 2** and the measured saturation profiles in Fig. 1.

Primary Drainage, Results. The calculated capillary pressure as well as the relative permeabilities to oil and water for the drainage case are shown in **Figs. 2 and 3**.

The resulting match of the steady-state water saturation profile and the transient total pressure drop are shown in **Figs. 4 and 5**. Good agreement exists between the calculated and measured saturation profiles. For the pressure drop some deviations exist but the general curve shapes are similar.

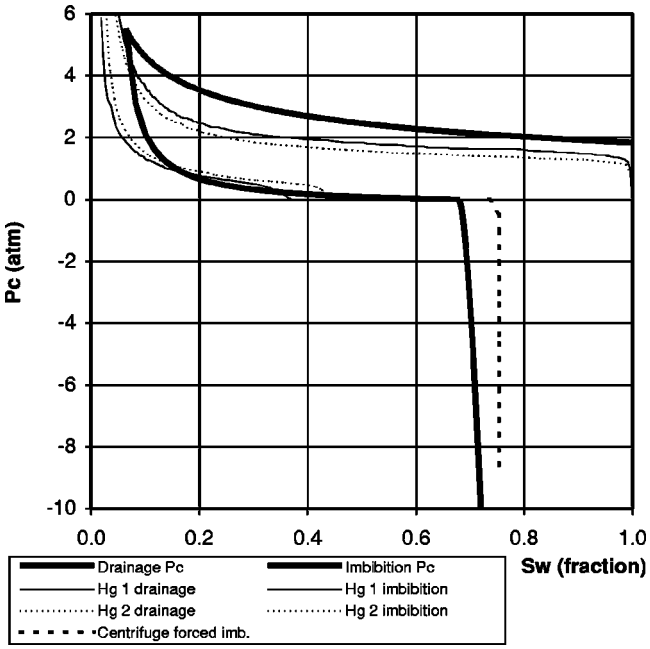

Fig. 2– Measured and calculated capillary pressure functions for sample M113.

Imbibition, Results. The calculated imbibition capillary pressure and relative permeability to oil are shown in Figs. 2 and 3. The scanning parameter was estimated to be 0.0375. The resulting match of the steady-state water saturation profile following the reversal of the oil flow direction is shown in Fig. 4. The general curve shape is predicted well. This is, however, not the case with the transient pressure drop during the reverse waterflooding, **Fig. 6**. The calculated pressure drop is smaller than the measured one. The reason for this behavior is not clear. It may be that the relative permeability to water is overestimated for the upper part of the water saturation interval. This in turn could indicate that the assumption of no hysteresis in the water relative permeability does not hold. Another supplementary explanation could be that the functional form, Eq. 11, is not satisfactory. It might be better to

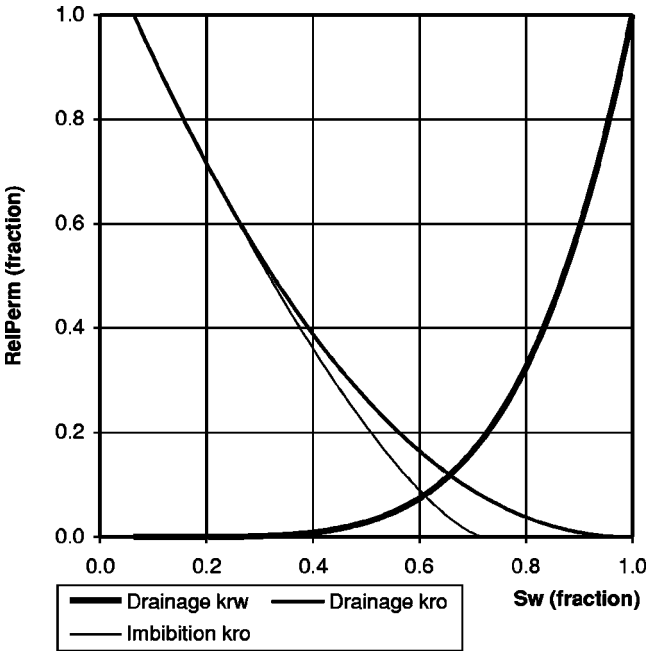

Fig. 3– Calculated relative permeability functions for sample M113.

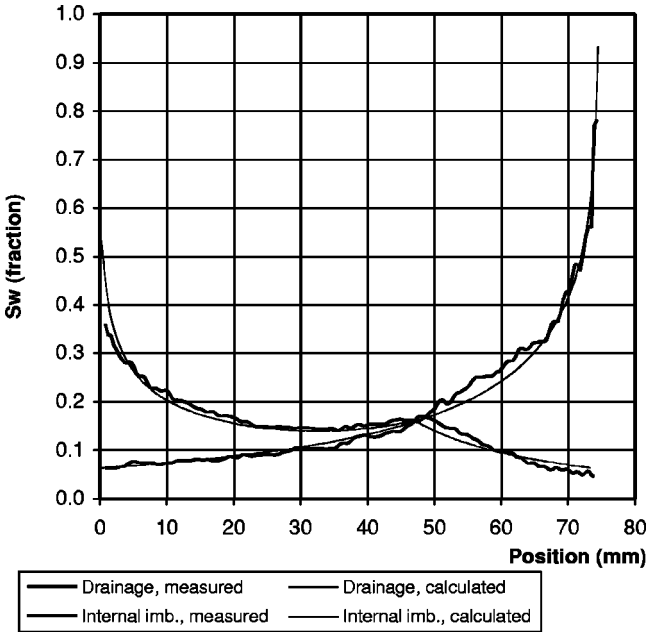

Fig. 4–Measured and calculated saturation profiles for sample M113.

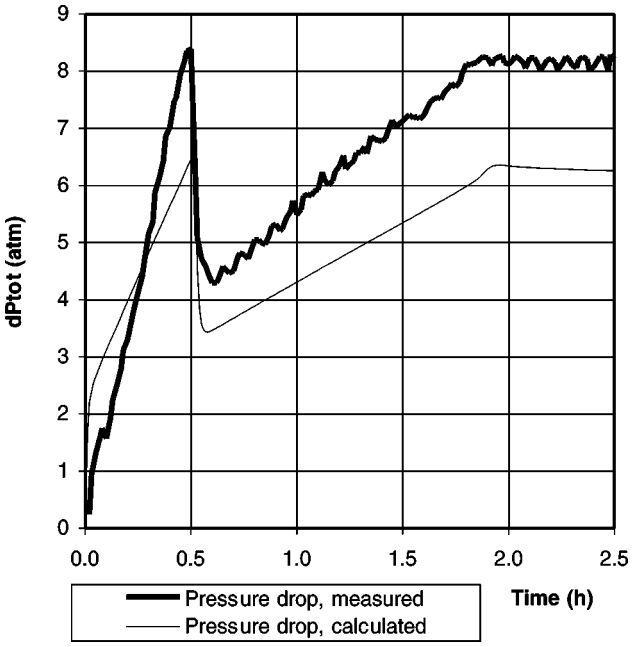

Fig. 6–Measured and calculated pressure drop for sample M113, forced imbibition case. At 0.5 h the flow rate was reduced from 10 to 5 mL/h.

use a combination of two different exponential functions, an exponential function and a straight line or perhaps *B* splines as suggested by Nordtvedt *et al.*[7] As pointed out by Kerig and Watson,[4] the exponential function is rather stiff. We have been using it here primarily to test the parameter estimation technique. In the future we will be looking for more flexible analytical representations of the relative permeabilities. At the same time, however, we will try to limit the number of unknowns as far as possible in order to reduce computation time as well as the risk of arriving at false solutions. A small objective function is no guarantee for a good solution.

The determined capillary pressure curves are compared with results obtained from a standard mercury injection technique and centrifuge method on the same plug, Fig. 2. The mercury injection curves are scaled by Leverett's *J* function using a standard value of 480 mN/m for the interfacial tension for the mercury/vapor system and a measured value of 38 mN/m for the oil/water system. No correction for contact angle is applied as the sample was strongly water-wet.[38] The drainage part of the capillary pressure curve is similar in shape to the mercury drainage curves, but the mercury injection data have a wider and more flat plateau. A similar situation has been reported previously.[19,39] The spontaneous part of the capillary pressure curve shows a significant deviation with respect to the mercury curves. The mercury injection technique gives a much lower capillary pressure at wetting-phase saturations below 0.15, together with a lower irreducible saturation. The lower irreducible saturation for the mercury injection technique may be caused by the high mercury drainage pressure, up to 2,000 bar. This may cause failure of the matrix as mercury penetrates into pore space, which previously was isolated for the nonwetting phase, as suggested by Christoffersen.[39] This may also explain the lower wetting-phase saturation obtained at $p_c=0$ for the mercury curves compared to the presented spontaneous capillary pressure curve. The forced imbibition capillary pressure curve compares reasonably well with a curve determined by the centrifuge technique, Fig. 2. The shape indicates strong wetting preference to water. This is also verified by the measured saturation profile for the waterflood, Fig. 1, which shows an almost uniform water saturation. The centrifuge data do show a lower oil residual saturation, which may be explained from the performance of the centrifuge experiment. The primary drainage of the centrifuge experiment was not completed, i.e., there was water production at the last pressure step applied in the centrifuge. Therefore, the oil residual saturation, for the centrifuge data, is obtained by scanning curves from an incomplete primary drainage process, which will give a saturation between $S_w=1.0$ and $S_w=1-S_{or}$.[36,40] A primary drainage capillary pressure curve could not be calculated from the centrifuge experiment, because the Hassler and Brunner calculation model[10] does not apply when water production has not ceased.

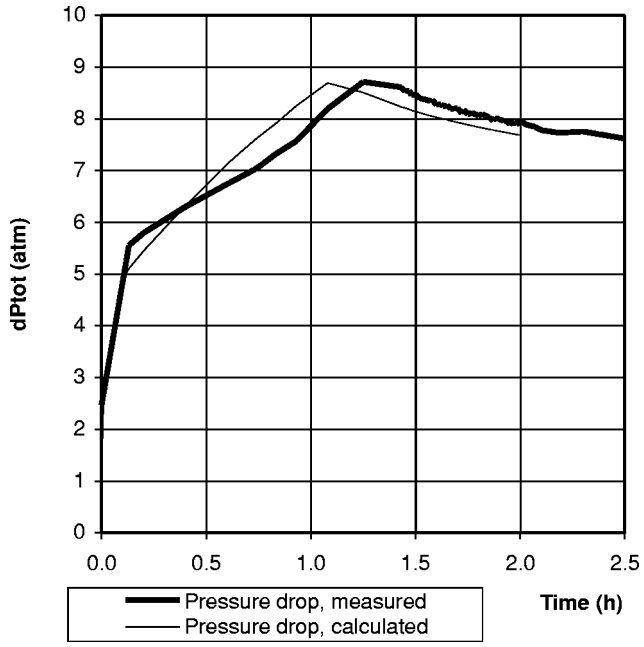

Fig. 5–Measured and calculated pressure drop for sample M113, drainage case.

Plug M16H. The M16H plug parameters and some experimental conditions are given in **Table 3**, and the measured saturation profiles in **Fig. 7**.

TABLE 3–PLUG M16*H* PARAMETERS	
$L = 73.4$ mm	$\mu_o = 0.92$ cp
$A = 1113$ mm^2	$S_{or} = 0.23$
$\phi = 0.333$	$S_{wi} = 0.05$
$k = 1.1$ md	$S_{w,apt} = 0.75$
$C_r = 1.76 \times 10^{-3}$ atm^{-1}	$p_{c,\max} = 4.708$ atm
$\rho_w = 1.049$ g/mL	$p_{o,\text{out}} = 1.0$ atm
$\mu_w = 1.12$ cp	$p_{th} = 1.678$ atm
$C_w = 4.58 \times 10^{-5}$ atm^{-1}	$q_o^{dr} = 10.0$ mL/h
$\rho_o = 0.73$ g/mL	$q_o^{imb} = -25.0$ mL/h
$C_o = 1.16 \times 10^{-4}$ atm^{-1}	$q_w^{imb} = -10.0$ mL/h

Primary Drainage, Results. The calculated capillary pressure as well as the relative permeabilities to oil and water are shown in **Figs. 8 and 9**.

The resulting match of the steady-state water saturation profile and the transient total pressure drop are shown in **Figs. 10 and 11**.

The drainage capillary pressure curve for plug M16H is also compared to mercury data obtained on the same plug, Fig. 8. The results are very similar to plug M113.

Imbibition, Results. The calculated imbibition capillary pressure and relative permeability to oil are shown in Figs. 8 and 9. The scanning parameter was estimated to be 0.0265. The resulting match of the steady-state water saturation profile following the reversal of the oil flow direction is shown in Fig. 10. Again, the general curve shape is predicted well. This is, however, not the case with the transient pressure drop during the reverse waterflooding, **Fig. 12**. The calculated pressure drop is smaller than the measured one just as it was in the case of plug M113. This supports the possible explanation that the relative permeability to water is overestimated for the upper part of the water saturation interval either due to an unsatisfactory analytical representation or because the assumption of no hysteresis in the water relative permeability does not hold.

The determined capillary pressure curves are compared with data obtained from a standard mercury injection technique, Fig. 8. Again, the results are similar to those of plug M113.

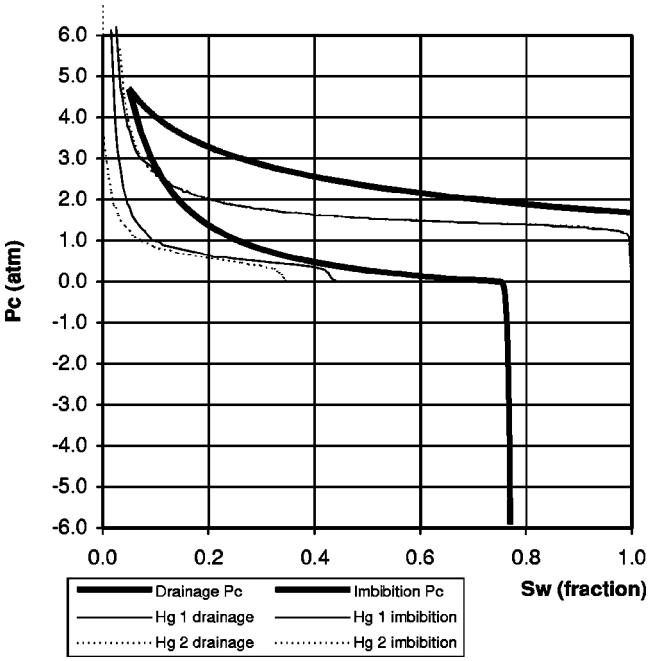

Fig. 8–Measured and calculated capillary pressure functions for sample M16H.

Conclusions

- A procedure to determine saturation functions for low-permeability rocks by a complex flooding procedure combined with a parameter estimation technique has been developed. The procedure utilizes the strong capillary retention of the wetting phase in such rocks. Capillary pressure functions and relative permeability functions, which are unbiased by capillary end effects, are produced for both drainage and imbibition situations.
- The procedure is based upon the following assumptions:
  1. The plug is homogeneous.
  2. The experiments reach a steady state.
  3. The analytical functions used are able to represent the saturation functions of the plug.

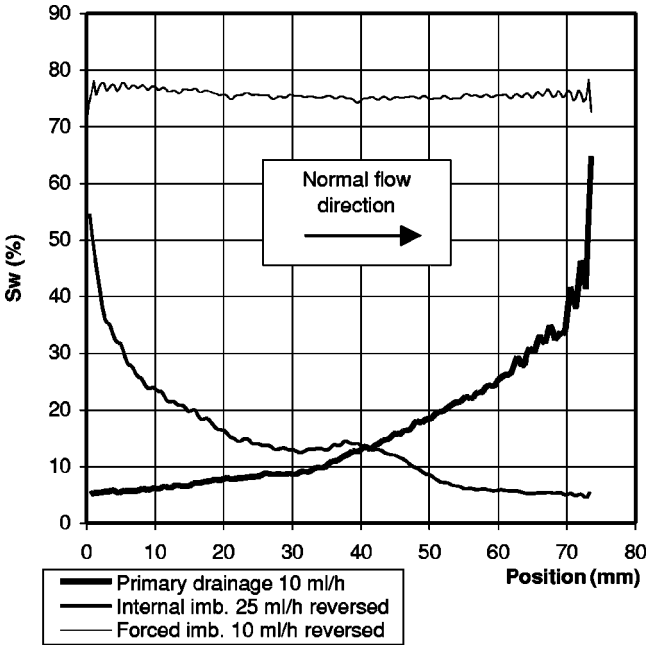

Fig. 7–Measured saturation profiles for sample M16H.

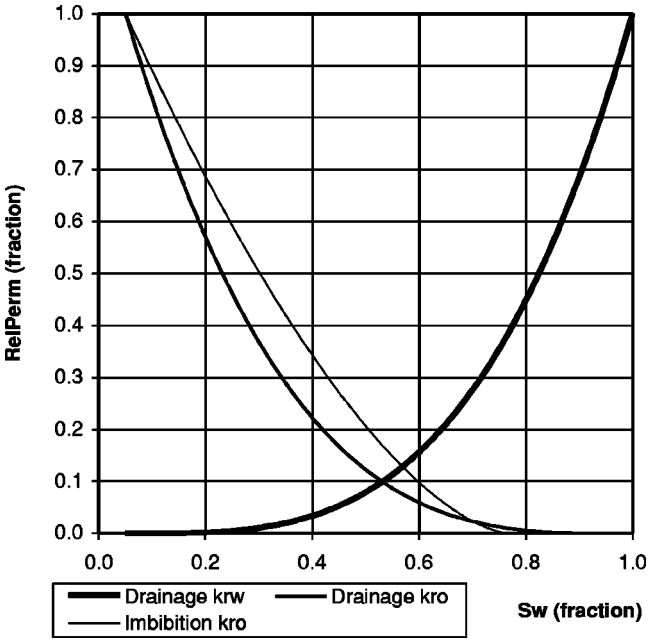

Fig. 9–Calculated relative permeability functions for sample M16H.

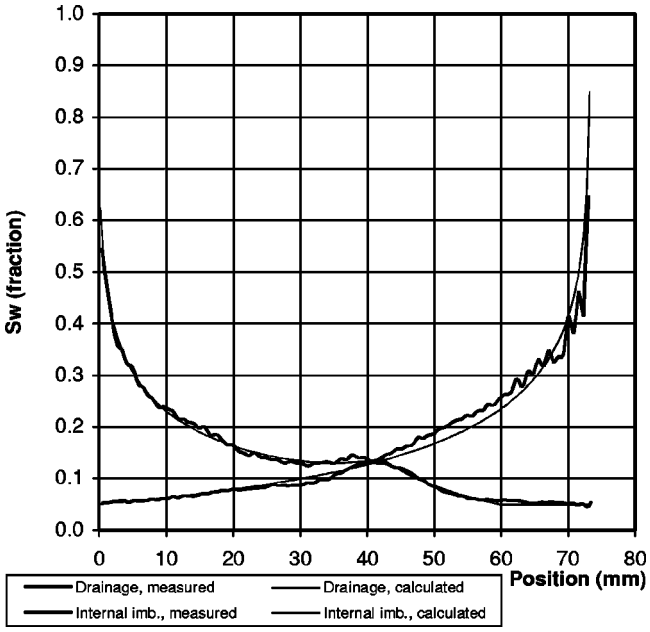

Fig. 10–Measured and calculated saturation profiles for sample M16H.

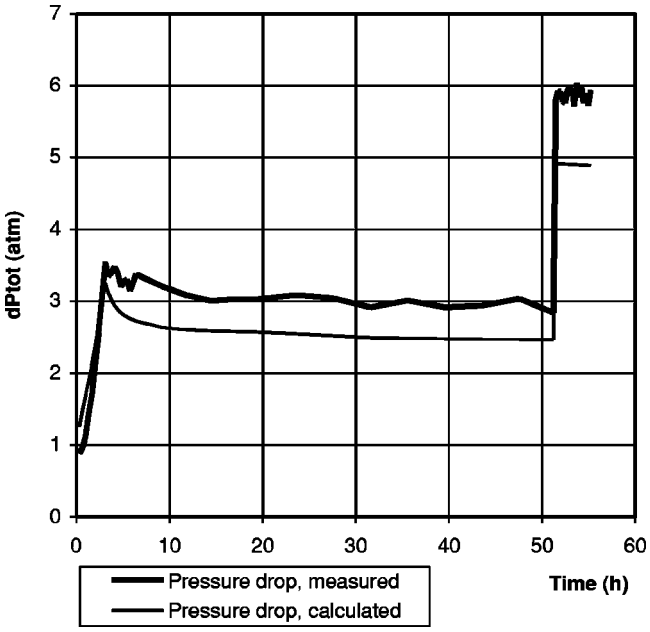

Fig. 12–Measured and calculated pressure drop for sample M16H, forced imbibition case. At 52 h the flow rate was increased from 5 to 10 mL/h.

- The procedure possesses the following advantages:
  1. The end effect is utilized and is, therefore, eliminated as a problem.
  2. The effects of oil and water relative permeabilities are separated.
  3. A consistent set of drainage and imbibition saturation functions are determined.
  4. Reservoir-like fluids can be used.
  5. The number of simultaneous unknowns is small (1 to 8).
- A complex five-step flooding procedure is presented from which information for calculation of both the drainage and imbibition part of the saturation functions is gained. The procedure utilizes a nonmagnetic core holder connected to a mobile flooding unit to allow saturation profile measurement in an NMR scanner, while the flooding is in progress.

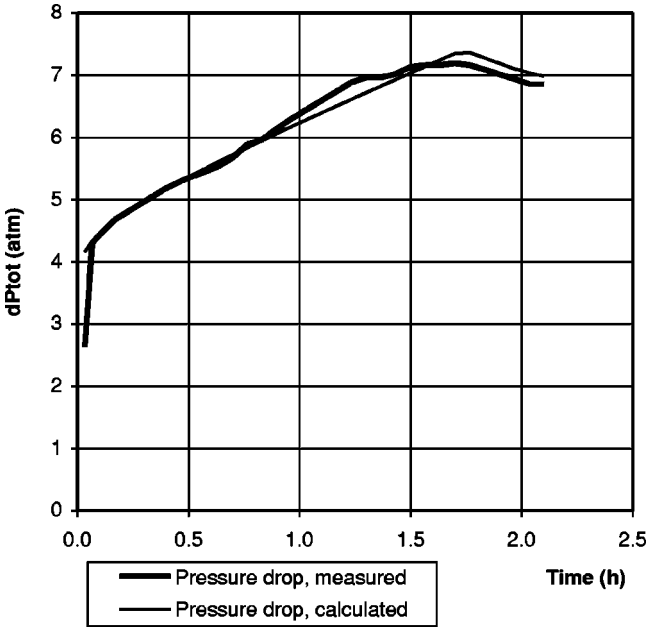

Fig. 11–Measured and calculated pressure drop for sample M16H, drainage case.

- Saturation profiles are obtained from a 4.7 T NMR scanner, with a one-dimensional chemical shift imaging pulse sequence. The mean accuracy of the pixel fluid saturations is better than 5 p.u., and reproducibility of pixel fluid saturations is better than 2 p.u. The accuracy of the mean fluid saturation of a sample is 2 p.u.
- The drainage saturation functions are calculated from a measured saturation profile, the pressure drop across the sample, and the threshold pressure obtained during a primary drainage process. The calculated drainage capillary pressure curves for two chalk samples are compared with scaled mercury injection data obtained from the same samples. The plateaus of the mercury data are consistently located at significantly lower capillary pressures. It is tentatively suggested that the mercury capillary data are invalidated by the highly aberrant surface tension and contact angle of the mercury/vacuum system, compared to an oil/brine system, and by destruction of the chalk pore structure by the high-pressure injection of mercury. Drainage relative permeabilities for the same two samples are calculated, but no independent verification is available.
- The imbibition saturation functions are calculated from measured saturation profiles and the pressure drop across the sample during two imbibition processes. The calculated spontaneous imbibition capillary pressure curve for two chalk samples are compared with scaled mercury injection data obtained from the same sample. Again, it is found that the plateaus of the mercury data are located at significantly lower capillary pressures, and in addition, the crossover points $p_c = 0$ are located at a much lower wetting-phase saturation. The suggestion of invalid mercury results is advanced as for the drainage case. Contrary to the mercury data, the forced imbibition capillary pressure curve for a centrifuge experiment is found to be in fair agreement with the results.
- The parameter estimation technique determines the capillary pressure scanning parameter ϵ. The determination presented here is based on Killough's method.
- In the present procedure, it is assumed that the relative permeability to water does not exhibit hysteresis. There is some indication that hysteresis is present. For both plugs considered, the measured forced imbibition pressure drop was underestimated using drainage water relative permeabilities. It may be an improvement to include a determination of the imbibition relative permeability to water in the parameter estimation technique.

• The wettability of a sample can be obtained directly from the set of capillary pressure curves.

Nomenclature

a = pore size, μm or coefficient
$\overline{a}$ = parameter vector
A = flow area, mm^2
b = coefficient
$\overline{b}$ = parameter vector
B_0 = main magnetic field, T
c = coefficient
$\overline{c}$ = parameter vector
C = Compressibility, atm^{-1}
e_1 = parameter in the analytical expression of the imbibition capillary pressure
e_2 = parameter in the analytical expression of the imbibition capillary pressure, atm
e_3 = parameter in the analytical expression of the imbibition capillary pressure
e_4 = parameter in the analytical expression of the imbibition capillary pressure, atm
e_5 = parameter in the analytical expression of the imbibition capillary pressure
E = noise level
f_a = analytical representation of the oil relative permeability
f_b = analytical representation of the capillary pressure, atm
f_c = analytical representation of the water relative permeability
f_1 = parameter in the analytical expression of the drainage capillary pressure, atm
f_2 = parameter in the analytical expression of the drainage capillary pressure
f_3 = parameter in the analytical expression of the drainage capillary pressure, atm
F_w = weight factor
J = objective function
k = absolute permeability, md
k_{ro} = relative permeability to oil, fraction
k_{rw} = relative permeability to water, fraction
L = length of core sample, mm
M = magnetization or number of squared saturation residuals
N = number of squared pressure drop residuals
p = pressure, atm
p_c^0 = $p_c(S_w^0)$
P = probability density function
q = flow rate, ml/h
S = fluid saturation, fraction
S_{or} = oil residual saturation, fraction
S_{iw} = irreducible water saturation, fraction
S^* = scaled saturation
S_w^0 = defined by Eqs. 16 and 17
t = time, hours
t_e = echo time, ms
t_r = repetition time, ms
T_1 = spin-lattice constant, ms
T_2 = spin-spin constant, ms
x = direction of flow downstream, mm
ϵ = scanning parameter
ϕ = porosity, fraction
μ = viscosity, cp
ρ = density, g/mL
ρ_p = proton density relative to distilled water, mol/L

Subscripts

c = capillary pressure
forced = forced imbibition
in = inlet of core sample
nc = number of coefficients (capillary pressure)
no = number of coefficients (relative permeability to oil)
nw = number of coefficients (relative permeability to water)
o = oil
out = outlet of core sample
spt = spontaneous imbibition
T = total
th = capillary threshold
w = water

Superscripts

C = calculated
dr = drainage
imb = imbibition
m = measured

Acknowledgments

The Danish Research Center of Magnetic Resonance is acknowledged for providing access to the 4.7 T SISCO NMR scanner. The Danish Ministry of Environment and Energy is acknowledged for funding part of the present work through the EFP-96 program.

References

1. Kulkarni, R.N., *et al.*: ''Estimation of Multiphase Flow Functions from Dynamic Displacement Data: Applications of NMR Imaging,'' paper SPE 36855 presented at the 1996 SPE European Petroleum Conference, Milan, Italy, 22–24 October.
2. Kohhedee, J.A.: ''Simultaneous Determination of Capillary Pressure and Relative Permeability of a Displaced Phase,'' paper SPE 28827 presented at the 1994 European Petroleum Conference, London, 25–27 October.
3. Chardaire-Riviére, C. *et al.*: ''Simultaneous Estimation of Relative Permeabilities and Capillary Pressure,'' *SPEFE* (December 1992) 283.
4. Kerig, P.D. and Watson, A.T.: ''Relative-Permeability Estimation From Displacement Experiments: An Error Analysis,'' *SPERE* (March 1986) 175; *Trans.*, AIME, **281**.
5. Watson, A.T. *et al.*: ''A Regression-Based Method for Estimating Relative Permeabilities From Displacement Experiments,'' *SPERE* (August 1988) 953.
6. Richmond, P.C. and Watson, A.T.: ''Estimation of Multiphase Flow Functions From Displacement Experiments,'' *SPERE* (February 1990) 121.
7. Nordtvedt, J.E., *et al.*: ''Determination of Three-Phase Relative Permeabilities From Displacement Experiments,'' *SPEFE* (December 1997) 221.
8. Ramakrishnan, T.S. and Capiello, A.: ''A New Technique to Measure Static and Dynamic Properties of a Partially Saturated Porous Medium,'' *Chem. Eng. Sci.* (1991) **46**, No. 4, 1157.
9. Fordham, E.J. *et al.*: ''Saturation Gradients in Drainage of Porous Media: NMR Imaging Measurements,'' *AIChE. J.* (1993) **39**, No. 9, 1431.
10. Hassler, G.L. and Brunner, E.: ''Measurement of Capillary Pressures in Small Core Samples,'' *Trans.*, AIME (1945) **160**, 114.
11. Christensen, R.L.: ''Geometric Concerns for Accurate Measurement of Capillary Pressure Relationships With Centrifuge Methods,'' *SPEFE* (December 1992) 311; *Trans.*, AIME, **293**.
12. Forbes, P.L., Chen, Z.A., and Ruth, D.W.: ''Quantitative Analysis of Radial Effects on Centrifuge Capillary Pressure Curves,'' paper SPE 28182 presented at the 1994 SPE Annual Technical Conference and Exhibition, New Orleans, 25–28 September.
13. Forbes, P.: ''Centrifuge Data Analysis Techniques: An SCA Survey on the Calculation of Drainage Capillary Pressure Curves from Centrifuge Measurements,'' SCA paper 9714 presented at the 1997 International Symposium of the Society of Core Analysis, Calgary, Alberta, Canada, 8–10 September.
14. Nielsen, C.M. *et al.*: ''Determination of Saturation Functions of Tight Core Samples Based on Measured Saturation Profiles,'' paper SCA 9721 presented at the 1997 International Symposium of the Society of Core Analysts, Calgary, Alberta, Canada, 8–10 September.
15. Olsen, D. *et al.*: ''Quantitative 1D Saturation Profiles on Chalk by NMR,'' *Magn. Reson. Imaging* (1996) **14**, No. 7/8, 847.
16. Nicholls, C.I. and Heaviside, J.: ''Gamma Ray Absorbtion Techniques Improve Analysis of Core Displacement Tests,'' paper SPE 14421 presented at the 1985 SPE Annual Technical Conference and Exhibition, Las Vegas, Nevada, 22–25 September.
17. Hicks, P.J.: ''X-Ray Computer-Assisted Tomography for Laboratory Core Studies,'' *JPT* (December 1996) 1120.

18. Honarpour, M.M., Huang, D.D., and Dogru, A.H.: ''Simultaneous Measurements of Relative Permeability, Capillary Pressure, and Electrical Resistivity with Microwave System for Saturation Monitoring,'' paper SPE 30540 presented at the 1995 SPE Annual Technical Conference and Exhibition, Dallas, 22–25 October.
19. Nørgaard, J.V., *et al.*: ''Capillary Pressure Curves for Low Permeability Chalk Obtained by NMR Imaging of Core Saturation Profiles,'' paper SPE 30605 presented at the 1995 SPE Annual Technical Conference and Exhibition, Dallas, 22–25 October.
20. Halperin, W.P. *et al.*: ''Magnetic Resonance Relaxation Analysis of Porous Media,'' in *Molecular Dynamics in Restricted Geometries*, J. Klafter and J.M. Drake (eds.), John Wiley & Sons, New York City (1989) 311.
21. Edelstein, W.A., *et al.*: ''NMR Imaging for Core Analysis,'' paper SPE 18272 presented at the 1988 Annual Technical Conference and Exhibition, Houston, 2–5 October.
22. Chen, S. *et al.*: ''NMR Imaging of Multiphase Flow in Porous Media,'' *AIChE. J.* (1993) **39**, 925.
23. Kulkarni, R. and Watson, A.T.: ''Robust Technique for Quantification of NMR Imaging Data,'' *AIChE. J.* (1997) **43**, No. 8, 2137.
24. Chen, S., Qin, F., and Watson, A.T.: ''Determining Fluid Saturations During Multiphase Flow Experiments by NMR Imaging Techniques,'' *AIChE. J.* (1994) **40**, No. 7, 1238.
25. Kim, K. *et al.*: ''Use of NMR Imaging for Determining Fluid Saturation Distributions During Multiphase Displacement in Porous Media,'' paper SCA 9219 (1992).
26. Kenyon, W.E. *et al.*: ''A Three-Part Study of NMR Longitudinal Relaxation Properties of Water-Saturated Sandstones,'' *SPEFE* (September 1988) 622.
27. Kleinberg, R.L. *et al.*: ''Nuclear Magnetic Resonance of Rocks: T_1 vs T_2,'' paper SPE 26470 presented at the 1993 SPE Annual Technical Conference and Exhibition, Houston, 3–6 October.
28. Howard, J.J.: ''Nuclear Magnetic Resconance Measurements of Wettability and Fluid Saturations in Chalk,'' 1994 EAPG/AAPG Special Conference on Chalk, Copenhagen, Denmark, 7–9 September.
29. Brownstein, K.R. and Tarr, C.E.: ''Importance of Classical Diffusion in NMR Studies of Water in Biological Cells,'' *Phys. Rev. A* (1979) **19**, No. 6, 2446.
30. Banavar, J.R. and Schwartz, L.M.: ''Probing Porous Media with Nuclear Magnetic Resonance,'' in *Molecular Dynamics in Restricted Geometries*, J. Klafter and J.M. Drake (eds.), John Wiley & Sons, New York City (1989) pp. 273–309.
31. Bech, N., Olsen, D., and Nielsen, C.M.: ''Determination of Oil/Water Saturation Functions of Chalk Core Plugs From Two-Phase Flow Experiments,'' paper SPE 49325 prepared for presentation at the 1998 SPE Annual Technical Conference and Exhibition, New Orleans, 27–30 September.
32. Madsen, K., Hegelund, P., and Hansen, P.C.: ''Nongradient Subroutines for Nonlinear Optimization,'' 1991 Report Ni-91-05, Institute for Numerical Analysis, Technical University of Denmark, June.
33. *ECLIPSE 100*, 95A Release, Intera Information Technologies, Ltd., Highlands Farm, Henley-on-Thames, Oxfordshire, U.K. (1994).
34. Frandsen, P.E.: ''SIMPE—Small Interface Module for Parameter Estimation,'' Geological Survey of Denmark and Greenland Report (1998) p. 61.
35. Braun, E.M. and Holland, R.F.: ''Relative Permeability Hysteresis: Laboratory Measurements and a Conceptual Model,'' *SPERE* (August 1995) 222.
36. Killough, J.E.: ''Reservoir Simulation With History-Dependent Saturation Functions,'' *SPEJ* (February 1976) 37; *Trans.*, AIME, **261**.
37. Olsen, D., Bech, N., and Nielsen, C.M.: ''Determination of Saturation Functions and Wettability for Chalk Based on Measured Fluid Saturations,'' Geological Survey of Denmark and Greenland Report (1998) p. 30.
38. Anderson, W.G.: ''Wettability Literature Survey—Part 4: Effects of Wettability on Capillary Pressure,'' *JPT* (October 1987) 1283.
39. Christoffersen, K.R.: ''High-Pressure Experiments With Application to Naturally Fractured Chalk Reservoirs, 1. Constant Volume Diffusion, 2. Gas-Oil Capillary Pressure,'' PhD dissertation, University of Trondheim (1992) 214 pp.
40. Aziz, K. and Settari, A.: ''Petroleum Reservoir Simulation,'' Elsevier Applied Science Publishers, Ltd., U.K. (1979).

SI Metric Conversion Factors

cp	×	1.0*	E−03	= Pa·s
md	×	9.869 233	E−16	= m^2
mL/h	×	2.778	E−10	= m^3/s
atm	×	1.013 250*	E+05	= Pa

*Conversion factors are exact.

SPEREE

Niels Bech is a senior researcher in the Dept. of Reservoir Geology at the Geological Survey of Denmark and Greenland (GEUS) in Copenhagen, Denmark. e-mail: nbe@geus.dk. He has worked for more than 13 years with the development and application of reservoir simulators. Bech holds an MS degree in electronic engineering and numerical mathematics from the Technical U. of Denmark. **Dan Olsen** is a senior petrophysicist at the Geological Survey of Denmark and Greenland. e-mail: do@geus.dk. He has worked with the application of NMR imaging and X-ray CT imaging to core analysis since 1989, primarily with measurement of spatially resolved fluid flow, fluid saturation, and porosity in core samples. Olsen holds an MS degree in petrology from the U. of Copenhagen. **Carsten Møller Nielsen** is a petrophysicist at the Geological Survey of Denmark and Greenland. His research interests are fluid flow in porous media and NMR. He holds an MS degree in chemical engineering from the Technical U. of Denmark